

An Online Spatial-Temporal Graph Trajectory Planner for Autonomous Vehicles

Jilan Samiuddin, Benoit Boulet and Di Wu

Abstract—The autonomous driving industry is expected to grow by over 20 times in the coming decade and, thus, motivate researchers to delve into it. The primary focus of their research is to ensure safety, comfort, and efficiency. An autonomous vehicle has several modules responsible for one or more of the aforementioned items. Among these modules, the trajectory planner plays a pivotal role in the safety of the vehicle and the comfort of its passengers. The module is also responsible for respecting kinematic constraints and any applicable road constraints. In this paper, a novel online spatial-temporal graph trajectory planner is introduced to generate safe and comfortable trajectories. First, a spatial-temporal graph is constructed using the autonomous vehicle, its surrounding vehicles, and virtual nodes along the road with respect to the vehicle itself. Next, the graph is forwarded into a sequential network to obtain the desired states. To support the planner, a simple behavioral layer is also presented that determines kinematic constraints for the planner. Furthermore, a novel potential function is also proposed to train the network. Finally, the proposed planner is tested on three different complex driving tasks, and the performance is compared with two frequently used methods. The results show that the proposed planner generates safe and feasible trajectories while achieving similar or longer distances in the forward direction and comparable comfort ride.

Index Terms—Autonomous driving, graph neural network, online trajectory planner, spatial, temporal

I. INTRODUCTION

Autonomous vehicles have the potential to improve overall transportation mobility in terms of safety and efficiency. The module which is primarily responsible for planning safely the motion of the vehicle through traffic is the trajectory planner. The trajectory planner is a vast and long-researched area using a wide variety of methods such as different optimization techniques, artificial intelligence and machine learning [1]. In this work, we propose a novel online trajectory planner by structuring the motion planning problem as sequences of spatial-temporal graphs passing through a sequential graph neural network architecture.

Manuscript received ; revised ; accepted ; This work was supported by Quebec's Fonds de recherche Nature et technologies. (Corresponding authors: Jilan Samiuddin, Di Wu.) The authors are with the Intelligent Automation Lab of the Centre for Intelligent Machines and the Department of Electrical and Computer Engineering, McGill University, Montreal, QC H3A 0E9, Canada (email: jilan.samiuddin@mail.mcgill.ca, benoit.boulet@mcgill.ca, di.wu5@mcgill.ca).

TABLE I: Nomenclature

| Symbol | Description | Symbol | Description |
|-----------------------|--|-------------------------|---|
| s, d | Longitudinal, lateral positions | V_s, V_d | Longitudinal, lateral virtual nodes |
| N_V | Number of virtual nodes | a, \ddot{s}, \ddot{d} | Acceleration and/or deceleration |
| v, \dot{s}, \dot{d} | Velocity | J | Jerk |
| U_o, U_v | Obstacle potential, velocity potential | y | Output vector of longitudinal and lateral positions |
| E | Ego vehicle | A | Actor vehicle |
| G | Graph | t_s | Sampling period |
| N | Planning Horizon | N_A | Number of actors |
| h | Feature or node embedding | W, B | Weights, biases |
| p, q | Target node, neighboring node | α | Attention coefficient |
| Subscript/Superscript | | | |
| acc, dec | Acceleration , Deceleration | upper, lower | Upper bound, lower bound |
| rec, safe | Recommended, safety | long, lat | Longitudinal, Lateral |

Different approaches have been undertaken by researchers to generate feasible trajectories. Sampling-based planners like the Rapidly-exploring Random Tree (RRT) has also been extensively tested on automated vehicles for online path planning [2] due to ease of incorporating user-defined objectives. Another sampling-based technique, state lattice [3, 4], discretizes the state space in a deterministic manner. Although the spatial-temporal version of the state lattice allows for planning with dynamic obstacles, its performance depends on sampling density, making it time-consuming [5]. However, the resulting paths from graph search-based planners and sampling-based planners are usually not continuous and thus jerky [6]. Interpolating curve planners are also popular choices, e.g., clothoid curves [7], polynomial curves [8], Bezier curves [9], etc. However, these planners require global waypoints defined and can be time-consuming when managing obstacles in real-time [6]. Frenet trajectory planners are also in the family of interpolating curve planners to generate optimal trajectory but utilize the Frenet coordinate frame instead of the Cartesian coordinate frame [10]. Geisslinger et al. [11] use the Frenet planner to generate candidate trajectories for an ego and then select the best candidate based on five different ethical principles in line with the European Commission (EU).

Graph-based approaches are also commonly found in the literature. These approaches encompass spatial or spatial-temporal representations, whether one-dimensional or hierarchical, like a tree across the feasible driving area [12]. Each node of the graph has an associated cost, and the graph-based algorithms seek to identify the path, minimizing the cost between the adjacent nodes. Graph search-based planners

A* [13], hybrid A* [14], and variations of these techniques have been widely used. The 2007 DARPA Urban Challenge was won by the vehicle called Boss that utilized the Anytime D* algorithm [15]. In more recent work, Han et al. [16] used hybrid A* to find collision-free paths and further optimized the path using kinematic constraints. Many use one-layered graphs in the spatial dimensions with lateral targets along the road [17, 18]. Gu et al. [3] apply multiple layered graphs with linear edges along the road. The adjacent nodes, which result in the least cost, are then used for path optimization. McNaughton et al. [4] explore both spatial and temporal dimensions in real-time in the search of a minimal cost path in the graph. A multilayered graph-based trajectory planner is also proposed by [12], where the planning task for a racing environment is divided into offline and online components. The offline part creates multiple drivable trajectories by connecting nodes in the graph, and then, in real-time, the online part picks the least expensive global state in the scene.

Artificial potential field techniques allow us to define potential fields using potential functions (PFs) for obstacles, road structures and goals and then plan paths by moving in the descent direction of the field [19]. In [20], Noto et al. generate the reference path to satisfy the dynamic constraints and to move the vehicle in the descent direction of the PFs. Rasekhipour et al. [19] combine the power of model predictive controller to address dynamic constraints and, the power of PFs to address obstacles and road structures to generate trajectories for the ego. An online motion planner for vehicle-like robots proposed by Chen et al. [21] uses PFs to generate the initial path meeting road constraints. The path is then optimized as an unconstrained weighted objective function for curvature maintenance, obstacle avoidance, and speed profile. In our work, we propose personalized PFs for obstacle avoidance and maximum velocity, keeping with priority given to the former.

The usage of machine learning for motion planning also has its fair share in the literature. Sung et al. [22] use neural networks to learn a planner online from data created using off-the-shelf path planning algorithms. The results show that the paths generated by the neural networks were smoother in contrast to the original paths. Prediction and planning are combined in [23] which deploys a neural network to predict the future states of the surrounding vehicles (actors) and an initial strategy. These are then forwarded into an optimization-based differentiable motion planner to determine the final plan. Yang et al. [24] use a hybrid approach where the behavioural learning is done using deep reinforcement learning (DRL) and the planning is done using a Frenet planner. In [25], A Deep Deterministic Policy Gradient (DDPG) planner is presented to determine the optimal trajectory based on pre-defined initial and final states and dynamic constraints. However, no obstacle is considered in the environment, and it requires 40,000 iterations before a good-quality trajectory can be achieved. Hoel et al. [26] extend the AlphaGo Zero algorithm to a continuous state space domain without self-play and combined planning and learning for tactical decision-making in autonomous driving. [27] proposes a safety layer in its reinforcement learning (RL) framework that pilots the

exploration process by limiting actions to the safe subspace of the whole action space. These safe actions are determined by taking into account all the possible trajectories of the traffic participants.

In this article, we propose spatial-temporal graphs that incorporate virtual nodes positioned along the road. These virtual nodes are designed to meet the road boundary conditions as well as the kinematic constraints of the ego. The ego and its surrounding actors also are nodes in the graph. The graphs are processed through a network architecture containing sub-networks in series that generate the future plan for the ego. In contrast to most prior methods, this future plan can include one or more of the following driving behaviors: lane-keeping, lane-changing, car-following, and speed-keeping. Furthermore, a simple behavioral layer is introduced to command the kinematic constraints of the ego for different driving tasks. The trajectory planner is tested for different driving tasks, and the results obtained demonstrate a better performance trade-off compared to the two baselines used in this work.

The main contributions of this work are summarized as follows:

- 1) We propose a novel spatial-temporal graph that depicts the trajectory planning problem and incorporates road constraints and kinematic constraints.
- 2) We present a neural network architecture that can process the above-mentioned graph to generate future plan for the ego.
- 3) We introduce personalized PFs for the architecture to learn on.
- 4) We design a simple behavioral layer for defining kinematic constraints of the ego.

The rest of this article is organized as follows. Section II provides brief descriptions of the theoretical framework used in this work. The proposed Spatial-Temporal Graph (STG) Trajectory Planner is elaborated in Section III. In Section IV, we discuss the experimental setup and the results. Finally, Section V concludes the article.

II. THEORETICAL BACKGROUND

A. Graph Neural Network

Graphs are used as a means of illustrating real-world problems. More particularly, graphs can capture the interactions between agents and how these agents evolve because of their involvement in a neighborhood. The agents in a graph are called the nodes and the interactions between them are presented using edges. Graphs can be of two types: homogeneous and heterogeneous. Heterogeneous graphs, unlike homogeneous graphs, have nodes and/or edges that can have various types or labels associated with them, indicating their different roles or semantics. For example, in our work, the node representing the ego has four features while the nodes for the surrounding actors have two features requiring a heterogeneous graph representation to capture the interactions between them. Because of the differences in type and dimensionality, a single node or edge feature tensor is unable to accommodate all the node or edge features of the

graph [28]. The computation of messages and update functions is conditioned on node or edge type. There are PyTorch libraries that are available to process heterogeneous graphs, which are detailed in [28].

Neural networks that operate on graphs are called Graph Neural Networks (GNNs) [29]. For example, in node representations, the GNN maps nodes of a homogeneous graph to a matrix $\mathbb{R}^{n \times m}$, where, n is the number of nodes and m is the dimensionality of the features of the nodes. For node p , the GNN aggregates information from its neighbors (e.g. averages the messages from its neighbors) and then applies a neural network in several layers [30]:

$$h_p^{(i+1)} = \sigma \left(W_i \sum_{q \in \mathcal{N}(p)} \frac{h_q^{(i)}}{|\mathcal{N}(p)|} + B_i h_p^{(i)} \right), \quad (1)$$

$\forall i \in \{0, 1, \dots, L-1\}$, where, h is the embedding of a node, σ is a non-linear activation function, W_i and B_i are the weights and biases of the i^{th} layer, respectively, $\mathcal{N}(p)$ is the neighborhood of the target node p , and L is the total number of layers.

Graph Attention Network (GAT) [31] is a GNN that integrates attention so that the learning is focused on more relevant segments of the input. The network learns the importance (also called the attention coefficient e_{pq}) of the neighbors of a node as it aggregates information from them. The attention coefficient between the target node p and its neighbor q is computed by applying a common linear transformation \mathbf{W} to the features (\mathbf{h}) of both p and q , followed by a shared attentional mechanism (att) as follows:

$$e_{pq} = \text{att}(\mathbf{W}\mathbf{h}_p, \mathbf{W}\mathbf{h}_q) \quad (2)$$

A single-layered feed-forward neural network is used for att in [31]. To compare the neighboring nodes properly, e_{pq} is normalized using the softmax function:

$$\alpha_{pq} = \frac{\exp(e_{pq})}{\sum_{k \in \mathcal{N}(p)} \exp(e_{pk})} \quad (3)$$

For a detailed explanation of GAT, readers can refer to [31].

B. Frenet Coordinates

Frenet coordinate system [10] is used to describe the location of a point relative to a reference curve. More particularly, the Frenet coordinates s and d represent the longitudinal and the lateral distances of the point of interest with respect to the curve from a starting point. Figure 1a shows the Frenet coordinates inside a Cartesian coordinate frame with respect to a reference curve.

It is important to note that any road structure (curved, straight, etc.) in the Cartesian coordinate framework can be presented as a straight line in the Frenet coordinate framework, as shown in Figure 1b. Thus, presenting an autonomous driving task in the latter domain is much simpler. In this work, we use the Frenet coordinates as features. Furthermore, for this work, after the problem is translated in the Frenet domain, the basis of the new frame is shifted ($\{s, d\} \rightarrow \{s_E, d_E\}$) with respect to the ego as shown in Figure 1b. By applying this

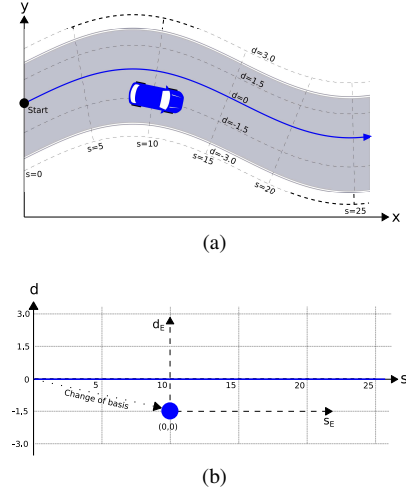


Fig. 1: (a) A snapshot of the road presented in the Cartesian coordinate frame showing the Frenet framework formulation with respect to the reference curve (in blue), and, (b) Frenet coordinate frame of the snapshot with the ego (blue circle). The new Frenet coordinate frame (black solid dashes) is with respect to the ego position

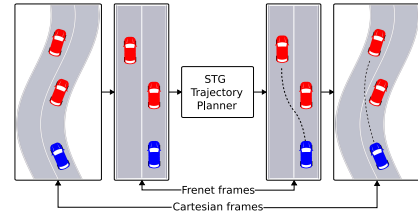


Fig. 2: Transformations between the Cartesian and the Frenet frames to obtain trajectory (in dashed line)

shift, it can be ensured that the magnitudes of the virtual nodes, as will be discussed in section III-B, always remain in a constrained range. Lastly, the Frenet coordinate frame also allows us to define the cost of a path very effectively based on the longitudinal and the lateral displacements of the ego and the other actors.

In this work, a scenario given in the Cartesian frame is first transformed into the Frenet frame, which is used to solve the trajectory problem using our proposed planner. The trajectory obtained in the Frenet frame is then transformed back to the Cartesian frame to get the actual trajectory for the ego. These steps are illustrated in Figure 2.

III. SPATIAL-TEMPORAL GRAPH (STG) TRAJECTORY PLANNER

In this section, the GNN-based trajectory planner utilizing a sequence of spatial-temporal graphs for trajectory planning is presented. For the formation of the planner, first, we discuss a simple behavioral layer that determines the kinematic constraints for the ego. Next, the formulation of the spatial graphs considering the road constraints, the kinematic constraints of the ego and the actors surrounding it are elaborated. Then, we present the network architecture that processes these graphs to obtain the future trajectory. Lastly, we define the cost function to be minimized by the network

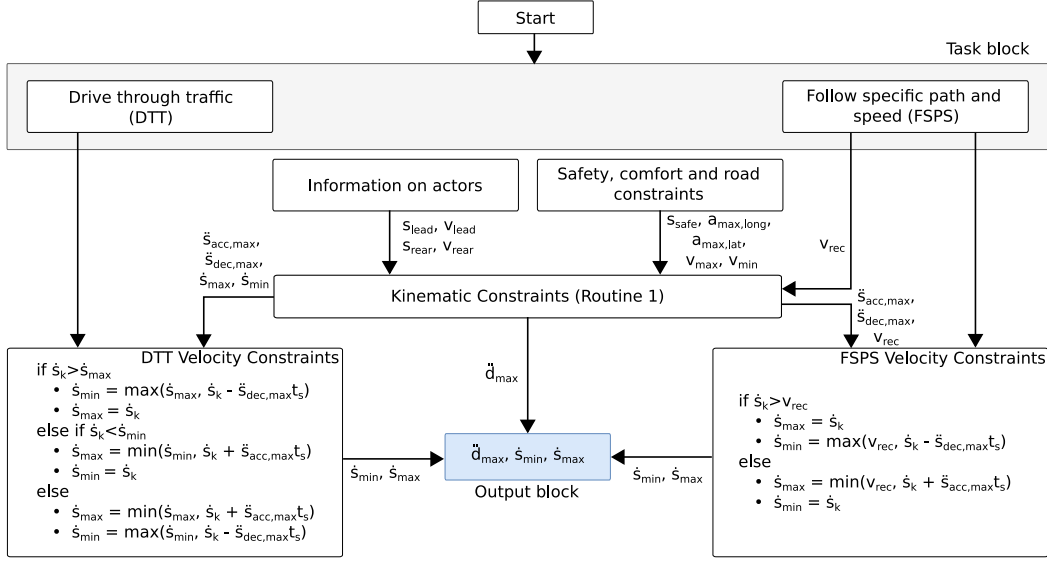


Fig. 3: Flow diagram for the behavioral layer (see Appendix for Routine 1)

for safety. Even though our work is on the design of the trajectory planner module, there are other vital modules in an autonomous vehicle system. Since the design of those other modules is out of the scope of this work, it is assumed that the states of the actors, road structure and the regulations are received from the perception module and the future states of the actors are received from the prediction module.

A. Behavioral Layer

In this section, we present a simple behavioral layer for our proposed framework – the design of a more sophisticated behavioral layer is out of the scope of this work. The behavioral layer determines kinematic constraints for the ego for different driving tasks, considering safety with respect to actors, comfort, and, road regulations. A kinematic constraint refers to a limitation or condition imposed on the vehicle’s motion based on its physical characteristics and the surrounding environment.

At first, parameters prioritizing safety (safety gap s_{safe}), comfort (the maximum longitudinal acceleration/deceleration $a_{max, long}$, the maximum lateral acceleration/deceleration $a_{max, lat}$) and road regulations (recommended speed v_{rec} if any, maximum road speed v_{max} , minimum road speed v_{min}) are defined. Next, the longitudinal gap with rear (s_{rear}) and/or lead (s_{lead}) actor(s), and its velocity (v_{rear} and/or v_{lead}) are identified. Note that a lead or a rear actor refers to actors which are immediate and are in the same lane as the ego. Using these parameters, the longitudinal and lateral kinematic constraints $\ddot{s}_{dec, max}$, $\ddot{s}_{acc, max}$, \dot{s}_{max} , \dot{s}_{min} , \ddot{a}_{max} and v_{rec} (see Table I for description) are obtained from Routine 1 (see Appendix). The behavioral layer, presented as a flow diagram in Figure 3, is designed to address two particular driving tasks: driving through traffic (DTT), and following a specific path and speed (FSPS). Using the updated constraints, the behavioral layer generates the longitudinal velocity constraints (\dot{s}_{max} , \dot{s}_{min}) and the lateral acceleration constraint (\ddot{a}_{max}) required in

the formulation of a spatial-temporal graph which will be discussed in the next subsection.

B. Spatial-Temporal Graphs

A self-driving vehicle must respect the road constraints, e.g., road/lane boundaries, speed limit, etc., to ensure safety. In addition, it cannot violate the kinematic constraints, e.g., steering limits, acceleration/deceleration limits. In our proposed formulation of the graph, we aim to incorporate some of these constraints. Note that the formation of the graphs requires knowledge of the future trajectories of the surrounding actors.

An example snapshot is depicted in Figure 4(a). In this snapshot, the ego is surrounded by three other actors. The ego is presented as the node E_k in the graph with its longitudinal and lateral positions and velocities as features at the k^{th} step with $k = 0, \dots, N - 1$, where N is the planning horizon and $k = 0$ denotes the initial timestamp. All of the N_A number of actors in a scenario are represented by nodes $A_{i, k+1}$ with $i = 1, \dots, N_A$. The future lateral and longitudinal positions of the actors at the $(k + 1)^{\text{th}}$ step are the features of their corresponding nodes. Next, we introduce the idea of virtual nodes V – these are imaginary points on the road spaced laterally or longitudinally – using kinematic constraints received from the behavioral layer as shown in Figure 4(b) – with respect to the ego as shown in Figure 4(c) and Figure 4(d), respectively. Thus, these virtualized nodes have only one feature – the lateral or the longitudinal spacing from the ego at k^{th} step. Note that the lateral and the longitudinal positions discussed are with respect to a reference path. In the remainder of the paper, we will use Frenet coordinates d and s for lateral displacement and longitudinal distances, respectively.

The lateral nodes are constrained by the road/lane boundaries and the lateral kinematic constraint \ddot{a}_{max} obtained from the behavioral layer. At the $(k + 1)^{\text{th}}$ step, the maximum

lateral velocity of the ego is given by

$$\dot{d}_{\max}^{k+1} = \ddot{d}_{\max} t_s \quad (4)$$

where, t_s is the sampling period. Therefore, equation (4) imposes the lateral kinematic constraints. The road constraint, i.e., $d_{\text{lower}} \leq d^{k+1} \leq d_{\text{upper}}$, where the boundary conditions d_{lower} and d_{upper} constrain the ego to stay on the road, is imposed using the following:

$$\begin{aligned} d_{\max}^{k+1} &= \min(d_{\text{upper}}, d^k + \dot{d}_{\max}^{k+1} t_s) \\ d_{\min}^{k+1} &= \max(d_{\text{lower}}, d^k - \dot{d}_{\max}^{k+1} t_s) \end{aligned} \quad (5)$$

where, d_{\max}^{k+1} and d_{\min}^{k+1} are the maximum and the minimum lateral distances that the ego can move. Given the number of lateral virtual nodes N_V , the nodes are layered laterally with equal spacing as follows:

$$\begin{aligned} V_{d,k+1} = [& d_{\min}^{k+1} & d_{\min}^{k+1} + \delta_d & d_{\min}^{k+1} + 2\delta_d & \dots \\ & d_{\max}^{k+1} - \delta_d & d_{\max}^{k+1} & &]^T \in \mathbb{R}^{N_V} \end{aligned} \quad (6)$$

where, δ_d is the spacing defined by

$$\delta_d := \frac{(d_{\max}^{k+1} - d_{\min}^{k+1})}{(N_V - 1)}. \quad (7)$$

For the longitudinal nodes, the kinematic constraints \dot{s}_{\max} and \dot{s}_{\min} obtained from the behavioral layer is applied. Thus, the maximum and the minimum longitudinal distances the ego can traverse are defined by

$$\begin{aligned} s_{\max}^{k+1} &= s^k + \dot{s}_{\max} t_s \\ s_{\min}^{k+1} &= s^k + \dot{s}_{\min} t_s, \end{aligned} \quad (8)$$

respectively. For N_V number of virtual longitudinal nodes, the longitudinal layering of these nodes are defined similarly as above:

$$\begin{aligned} V_{s,k+1} := [& s_{\min}^{k+1} & s_{\min}^{k+1} + \delta_s & s_{\min}^{k+1} + 2\delta_s & \dots \\ & s_{\max}^{k+1} - \delta_s & s_{\max}^{k+1} & &]^T \in \mathbb{R}^{N_V} \end{aligned} \quad (9)$$

where, δ_s is the equal spacing between the adjacent nodes defined by

$$\delta_s := \frac{(s_{\max}^{k+1} - s_{\min}^{k+1})}{(N_V - 1)} \quad (10)$$

After all the nodes (E_k , $A_{i,k+1}$, $V_{s,k+1}$ and $V_{d,k+1}$) have been defined, the graph G_k is formed as shown in Figure 4(e). The edges between E_k and $A_{i,k+1}$ are bidirectional signifying the “interactions” between the ego and the other actors – the edge features are the euclidean distances between the ego and the corresponding actors. The edges between the ego and the virtual nodes are unidirectional (E to V_s and V_d) signifying the transition from k^{th} to $(k+1)^{\text{th}}$ step (the temporal aspect of the graph itself). Thus, the edge attribute for the edges between E and V_s and V_d , is set to be the sampling period t_s . The lateral virtual nodes are connected by bidirectional edges to their adjacent nodes with each edge attribute being the corresponding lateral distance between the corresponding nodes. The interactions between the longitudinal nodes are formulated in the same manner.

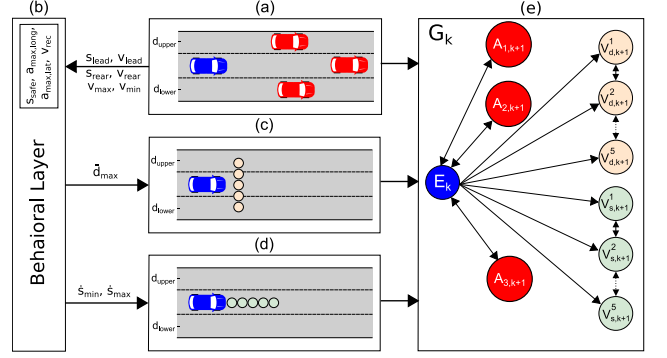


Fig. 4: (a) The ego (in blue) is surrounded by actors (in red). (b) The behavioral layer generates kinematic constraints for the current scenario. (c) The lateral virtual nodes (in light peach) is spread out laterally along the road, respecting road boundaries. (d) The longitudinal virtual nodes (in light green) are spread out longitudinally ahead of the ego along the road. (e) Formation of graph G_k for the given snapshot with $N_V = 5$

C. STG Network Architecture

The task of the STG network architecture is to output the future longitudinal and lateral positions of the ego. To do that, we utilize a GAT network [31] as an encoder to generate a node embedding of the spatial-temporal graph G_k (equation (11)) and create the encoded feature vector Φ_{GAT} (equations (12) and (13)). A multilayer perceptron (MLP) decoder with a fixed-size input further processes Φ_{GAT} to generate the decoded features Φ_{MLP} (equation (14)). A softmax function is then applied on Φ_{MLP} in two layers to compute two sets of weights Φ_{Softmax}^s and Φ_{Softmax}^d for the longitudinal and lateral virtual nodes, respectively (equation (15)). These weights determine the relative importance of the virtual nodes. Finally, inner products between the virtual nodes and the weights are computed to obtain the future position y_{k+1} of the ego at the $(k+1)^{\text{th}}$ step (equation (16)). Each of the mentioned sequential steps are further detailed below and shown in Figure 5.

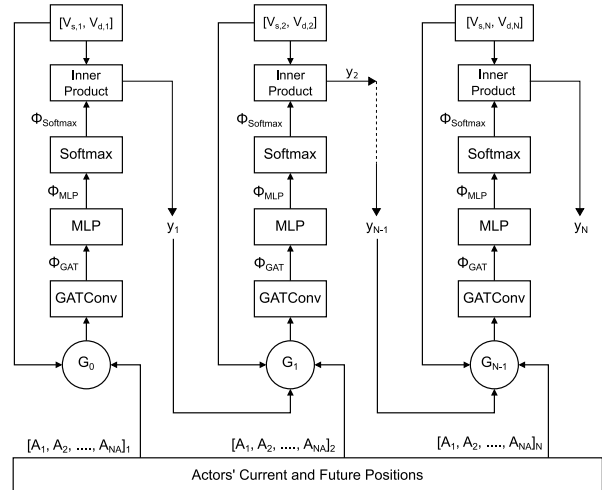


Fig. 5: Network architecture to learn online the future trajectory of the ego

The graph G_k that represents the snapshot of the ego's surrounding at the k^{th} step needs to be processed to identify the position of the ego at the $(k+1)^{\text{th}}$ step. In order to do so, we propose the framework shown in Figure 5. At first, G_k is passed through a GAT network that generates an embedding of size r for each of the nodes, i.e.,

$$\left[\Phi_{\text{GAT}}^E, \Phi_{\text{GAT}}^{V_s}, \Phi_{\text{GAT}}^{V_d}, \Phi_{\text{GAT}}^{A_1}, \dots, \Phi_{\text{GAT}}^{A_{N_A}} \right] = \text{GATConv}(G_k) \quad (11)$$

where, $\Phi_{\text{GAT}}^E \in \mathbb{R}^r$ for the ego, $\Phi_{\text{GAT}}^{V_s} \in \mathbb{R}^{N_V \times r}$ for the N_V longitudinal virtual nodes, $\Phi_{\text{GAT}}^{V_d} \in \mathbb{R}^{N_V \times r}$ for the N_V lateral virtual nodes, and $\Phi_{\text{GAT}}^{A_1}, \Phi_{\text{GAT}}^{A_2}, \dots, \Phi_{\text{GAT}}^{A_{N_A}} \in \mathbb{R}^r$ for the N_A actors. Note that the varying number of actors N_A surrounding the ego cause G_k to be a dynamic graph, i.e., addition and deletion of actor nodes from G_k .

Since MLPs expect a fixed-size input and the GAT network applied to G_k may have different sizes depending on N_A , we address this structural problem by applying graph pooling [32] on the actor nodes only:

$$\Phi_{\text{GAT}}^A = \Phi_{\text{GAT}}^{A_1} + \Phi_{\text{GAT}}^{A_2} + \dots + \Phi_{\text{GAT}}^{A_{N_A}} \quad (12)$$

such that $\Phi_{\text{GAT}}^A \in \mathbb{R}^r$. Graph pooling based on the sum is often adequate for applications involving small graphs as used in this work [32]. Finally, the output of the GAT network is generated by concatenation as follows:

$$\Phi_{\text{GAT}} = \text{concat} \left(\Phi_{\text{GAT}}^E, \Phi_{\text{GAT}}^A, \left(\Phi_{\text{GAT}}^{V_s} \right)^f, \left(\Phi_{\text{GAT}}^{V_d} \right)^f \right) \quad (13)$$

where, $\Phi_{\text{GAT}} \in \mathbb{R}^{2r+2rN_V}$ and the $(\cdot)^f$ operator is the flattening function [33] that returns an array collapsed into one dimension. With Φ_{GAT} as the input, the MLP decoder generates the decoded states as follows:

$$\Phi_{\text{MLP}} = \text{MLP}(\Phi_{\text{GAT}}) \in \mathbb{R}^{2N_V} \quad (14)$$

Note that the output size for the MLP decoder is set to $2N_V$ since the idea is to create weights for the N_V longitudinal nodes and the N_V lateral nodes by applying softmax function S . Then S is used to normalize Φ_{MLP} in two layers (first N_V elements of Φ_{MLP} for longitudinal weights and the remaining N_V elements for lateral weights) as follows:

$$\begin{aligned} \Phi_{\text{Softmax}}^s &= S \left(\Phi_{\text{MLP}}^{1:N_V} \right) \in \mathbb{R}^{N_V} \\ \Phi_{\text{Softmax}}^d &= S \left(\Phi_{\text{MLP}}^{N_V+1:2N_V} \right) \in \mathbb{R}^{N_V} \end{aligned} \quad (15)$$

Finally, the virtual lateral and longitudinal nodes are weighted using Φ_{Softmax}^d and Φ_{Softmax}^s to get the output

$$y_{k+1} = \left[\langle \Phi_{\text{Softmax}}^s, V_{s,k+1} \rangle \quad \langle \Phi_{\text{Softmax}}^d, V_{d,k+1} \rangle \right]^T \quad (16)$$

where, $y_{k+1} = \left[s^{k+1} \quad d^{k+1} \right]^T \in \mathbb{R}^2$ is a vector of the future longitudinal and lateral positions at the $(k+1)^{\text{th}}$ step, and, the operator $\langle \cdot \rangle$ represents the inner product. y_{k+1} is then utilized to obtain G_{k+1} and the same routine is followed to obtain y_{k+2} and so on as shown in Figure 5.

D. Potential Functions

The network needs to backpropagate some “loss” to learn. However, in an online trajectory planner, there is no labelled trajectory, and thus, no loss can be calculated. Therefore, we propose potential functions (PFs) of the obstacles that determine the safety of the ego for a given trajectory. The obstacle PF has a maximum value in its position to repel the ego.

For an actor longitudinally and laterally distanced from the ego by Δs and Δd , respectively, is assigned the longitudinal and the lateral potential functions as follows:

$$U^{\text{long}} := \frac{b_1}{(b_2 \Delta s + \varepsilon_1)^2} \quad (17)$$

$$U^{\text{lat}} := \frac{b_3 U^{\text{long}}}{(b_4 \Delta d + \varepsilon_1)^2} \quad (18)$$

respectively, where b_1, b_2, b_3, b_4 , and ε_1 are constants. Equation (17) – a slight variation of the repulsive potential proposed by [34] – simply indicates that maintaining a larger longitudinal distance alone is safer. However, safety with respect to lateral distance alone is not sufficient. An actor maintaining a particular lateral distance from the ego at a very close proximity in terms of the longitudinal distance possesses higher risk than an actor maintaining the same lateral distance but further away longitudinally. Thus, we propose equation (18) that accounts for this phenomenon and Figure 6(a) illustrates it. For N_A number of actors surrounding the ego, the total potential function of the obstacles U_o is determined as follows:

$$U_o := \sum_{i=1}^{N_A} U_i^{\text{lat}} \quad (19)$$

Next, it is important to realize that when the ego is driven through traffic, the planner network may slow the ego so that the surrounding actors can pass by suggesting a lower potential U_o . However, this is an ineffective way of solving the trajectory plan. Thus, to address the issue, a potential function of velocity U_v is also introduced in this work:

$$U_v := c_1 \left(\frac{c_2}{U_o + \varepsilon_2} \right)^{\frac{s_{\text{max}}}{s}} \quad (20)$$

where c_1, c_2 , and ε_2 are constants. Equation (20) implies that lower velocities should have higher potential when the risk is lower, i.e., U_o is lower. Thus, the velocity PF has its maximal value when the risk is the lowest and the ego is travelling at the minimum velocity. On the other hand, when U_o is higher, the velocity PF is minimal since safety is a higher priority. Figure 6(b) illustrates U_v . Finally, the total potential U_{total} (i.e., the “loss”) backpropagated into the network is given by

$$U_{\text{total}} = \sum_{k=0}^{N-1} (U_o^{k+1} + U_v^{k+1}) \quad (21)$$

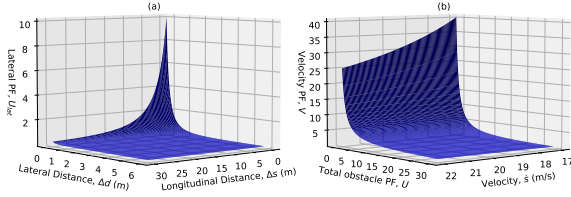


Fig. 6: Potential functions – (a) Lateral potential function, and, (b) Velocity potential function

IV. EXPERIMENTAL RESULTS AND ANALYSIS

A. Driving Tasks

In this section, some autonomous driving tasks are defined to evaluate the performance of the proposed planner. These tasks vary in complexity, e.g., vehicle following and lane keeping are on the simpler side of the spectrum, whereas, merging, and driving through traffic are at the other end [35]. Often, simpler tasks are sub-tasks of more complex tasks. Particularly, we define three complex problem statements – vehicle following and lane keeping are sub-tasks of the defined problems.

1) *Driving Through Traffic*: Aradi [35] suggests that driving through traffic is the most complicated setup to test a planner. Although this task is scalable, we limit the task to highway driving. Three different densities – low, medium, and high – of traffic scenarios (100 for each) were generated using the SL2015 model of SUMO (Simulation of Urban MObility) simulator [36]. The low-density traffic scenario consists of 1-5 actors, the medium-density traffic scenarios consist of 10-14 actors surrounding the ego, and the high ones consist of 15-20 actors surrounding the ego. The actors are set to respect the speed limits of the road. Once the traffic is generated, an agent from the scene is randomly selected to play the role of the ego while the trajectories of other agents remain unchanged. In this task, the ego has to plan a safe trajectory for a 5 seconds horizon with 0.1 second sampling time.

2) *Merging*: In this task, the ego (driving at 50 km/h) has to merge to a highway and its lane ends in approximately 100 m. The recommended speed to enter the merging lane is set at $v_{rec} = 60$ km/h. There is an actor approaching with a speed of 70 km/h in the merging lane of the highway. There is another actor in the adjacent lane driving at 75 km/h.

3) *Taking an Exit*: The ego currently driving at 80 km/h has to take an exit with the recommended speed of $v_{rec} = 50$ km/h. There is an actor approximately 25 m ahead of it driving at 55 km/h. In the course of time, the actor also takes the exit, reducing its speed to the recommended speed. Another actor is driving in the adjacent lane at 75 km/h, which does not take the exit.

B. Baselines

Two baselines are used in this paper to assess and compare our proposed technique. The kinematic constraints used in both baselines are the same used in the proposed method.

SL2015 from SUMO is used as the first baseline. The SL2015 model is a lane-changing behavior model used to replicate real-world lane-changing maneuvers in a traffic simulation. The model allows for the definition of kinematic

constraints such as the maximum lateral and longitudinal speeds. The model makes lane changing decisions based on several factors, such as the difference between the current and the desired speeds, cooperation between the driving agents, and the safety gap in the current lane. The data generated using the model already defines the trajectory of the randomly chosen agent as the ego. Thus, the trajectory not only respects the kinematic constraints but also mimics cooperative behavior with other actors on the road to maintain safety.

Next, we use the Frenet path planner from MATLAB (MFP) [37]. It generates multiple candidate trajectories using fourth or fifth-order polynomials relative to the reference path. The candidates are then pruned by checking for kinematic constraints. Next, the trajectories are assessed for collision against the predicted motions of the surrounding actors and the colliding ones are eliminated. Finally, the cost of the remaining trajectories is measured, and the least expensive trajectory is selected. Equation (21) is used for measuring the cost.

C. Evaluation Metrics

The trajectory qualities are evaluated in terms of safety, comfort and the longitudinal distance travelled. Safety is assessed by the proposed risk score shown in equation (19) as follows:

$$\text{Risk} = \frac{1}{T} \int_0^T U_o(t) dt, \quad (22)$$

where T is the planning horizon in seconds. Minimum jerk – the the time rate of change in acceleration – reflects maximal smoothness, and thus, the discomfort score can be defined using integrated absolute jerk [38]:

$$\text{Discomfort} = \frac{1}{T} \int_0^T |J(t)| dt, \quad (23)$$

where, $J = \sqrt{J_{long}^2 + J_{lat}^2}$ is the total jerk experienced in the trajectory in both longitudinal and lateral directions. The longitudinal distance is extracted from the trajectory itself.

D. Experimental Results

For the task of driving through medium and high density traffics, our STG planner achieved 100% success rate in planning feasible trajectories, i.e., trajectories that do not cause a collision and do not violate the kinematic constraints. However, MFP failed to find feasible trajectories in 27%, 29%, and 33% of the scenarios with low, medium, and high traffic, respectively. The SUMO2015 model being the basis to generate the trajectories, does not account for any failure. Table II shows the performance comparisons between the three planners for the driving through traffic task. The median score is presented for each of the metrics as it defines the central tendency. Note that the results for MFP shown in the table include only the scenarios where it succeeded.

For all types of traffic, MFP generates the most comfortable trajectories and the proposed planner stands second in the same aspect. However, the primary objective of a planner is the ability to find a feasible path, and our proposed STG planner demonstrates 100% success rate in planning

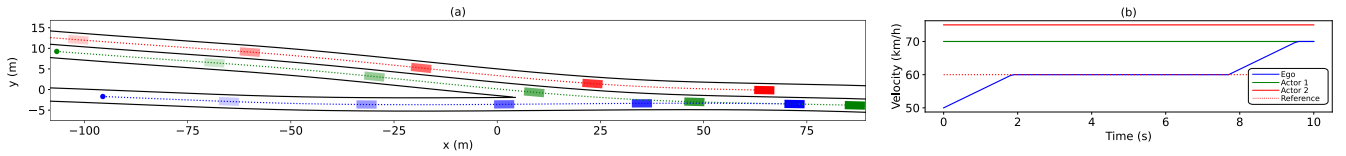


Fig. 7: (a) The ego (blue rectangle) merging into the highway from the start (dot) and the rectangles represent the progression of the vehicles over time spaced by 2 seconds. (b) The velocity profiles of the ego and the actors for the merging task

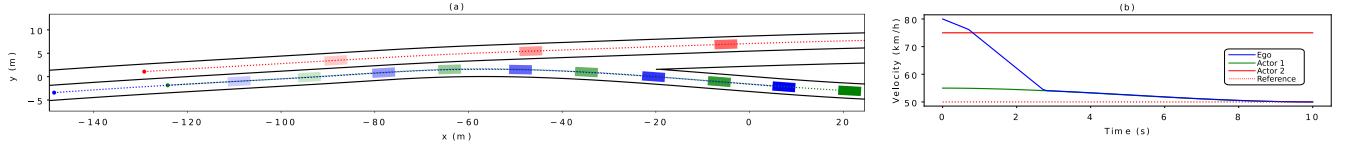


Fig. 8: (a) The ego (in blue) taking the exit and the rectangles represent the progression of the vehicles over time spaced by 2 seconds. (b) The velocity profiles of the ego and the actors for the exit task

TABLE II: Median score comparisons (best score in bold) between the proposed and the baselines (100 random scenarios for each type of traffic)

| Traffic Type | Planner | Discomfort [m/s ³] | Risk | Longitudinal Distance [m] |
|------------------------|---------|--------------------------------|-------------|---------------------------|
| Low density traffic | STG | 0.52 | 5.76 | 108.24 |
| | MFP* | 0.2 | 5.19 | 104.22 |
| | SL2015 | 2.41 | 5.81 | 109.58 |
| Medium density traffic | STG | 1.04 | 6.30 | 108.55 |
| | MFP** | 0.22 | 7.12 | 96.85 |
| | SL2015 | 2.26 | 10.24 | 96.98 |
| High density traffic | STG | 1.12 | 7.08 | 109.39 |
| | MFP*** | 0.26 | 7.42 | 97.92 |
| | SL2015 | 2.88 | 10.84 | 98.26 |

*73 feasible trajectories, **71, ***67

in contrast to MFP. In low-density traffic scenarios, MFP performs the best in terms of risk, while SL2015 performs the best in terms of longitudinal distance travelled. However, STG achieves a better risk score than SL2015 and has a better longitudinal distance travelled than MFP for the same traffic. The scores for medium and high-density the traffic shows that our planner achieves not only more longitudinal distance but also safer trajectories. MFP generates trajectories that are the shortest in terms of longitudinal distance, while SL2015 generates trajectories that are the least safe. Figure 7 shows the performance of STG in the merging task. The velocity profile shows that it accelerates to reach the recommended speed (60 km/h) to merge. It continues with the speed until it gets behind a lead actor (in green) and starts following it effectively. In the task of taking an exit, STG generates a safe trajectory, as well as shown in Figure 8. The ego starts to slow down but finds a lead actor (in green also taking the exit) and then follows it quite efficiently to take the exit. In both the above two tasks, STG demonstrates its efficacy in the following three sub-tasks: speed-keeping, car-following and lane-keeping.

E. Interpretability

The trained GAT network encapsulates the interactions between the nodes with an attention mechanism as explained in section II-A. Figure 9 shows the attention in equation (3) evolving over time between the ego and the actors in the tasks

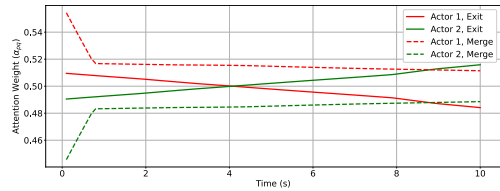


Fig. 9: α_{pq} between ego p and actor q

defined in sections IV-A2 and IV-A3. In the merging task, it can be seen that since both the actors are closing in and remain close, their attention values tend to converge towards each other. In the other task of taking an exit, the attention of the actor taking the exit ahead of the ego increases while the attention of the actor not taking the exit decreases. While it is difficult to explain the magnitude of these attention values, it is rather intuitive that the ego should have increasing focus on the actor taking exit along with it rather than the one going in another direction.

V. CONCLUSION

In this work, a novel online spatial-temporal graph trajectory planner is introduced. Heterogeneous graphs are used to formulate the problem by taking into account road boundaries and kinematic constraints. Then, these graphs are processed in a sequential neural network architecture to get the desired future trajectory that can depict common driving behaviors such as lane-keeping, lane-changing, car-following, and speed-keeping. For the network to learn, potential functions addressing safety and maximum velocity keeping are presented as well. In addition, a simple behavioral layer is presented to provide kinematic constraints for the planner. The results show that our proposed planner succeeded in generating feasible trajectories in all the driving tasks. In contrast to the baselines, the metrics point to better trade-off performance.

In the future, we want to test the efficacy of the proposed planner in more diverse driving tasks using more complex behavioral layers. We also plan to extend the application of our method to cooperative multi-agent connected autonomous driving.

APPENDIX

Routine 1 Pseudo code to obtain kinematic constraints

```

function Kinematic Constraints
Inputs:
     $s_{\text{lead}}, s_{\text{rear}}, v_{\text{lead}}, v_{\text{rear}}, a_{\text{max, long}}, v_{\text{max}},$ 
     $v_{\text{min}}, a_{\text{max, lat}}, v_{\text{rec}}, s_{\text{safe}}, \text{DTT}, \text{FSPS}$ 
Do:
1  if not( $s_{\text{lead}} < s_{\text{safe}}$  or  $s_{\text{rear}} < s_{\text{safe}}$ )
2       $\ddot{s}_{\text{dec, max}} = a_{\text{max, long}}$ 
3       $\ddot{s}_{\text{acc, max}} = a_{\text{max, long}}$ 
4       $\dot{s}_{\text{max}} = v_{\text{max}}$ 
5       $\dot{s}_{\text{min}} = v_{\text{min}}$ 
6       $\dot{d}_{\text{max}} = a_{\text{max, lat}}$ 

7  if  $s_{\text{lead}} < s_{\text{safe}}$ 
8       $\ddot{s}_{\text{dec, max}} = 2a_{\text{max, long}}$ 
9       $\dot{s}_{\text{max}} = v_{\text{lead}}$ 
10     if FSPS
11          $v_{\text{rec}} = v_{\text{lead}}$ 

12  if  $s_{\text{rear}} < s_{\text{safe}}$ 
13       $\ddot{s}_{\text{acc, max}} = 2a_{\text{max, long}}$ 
14       $\dot{s}_{\text{min}} = v_{\text{rear}}$ 
15      if FSPS and  $v_{\text{rec}} < \dot{s}_{\text{min}}$ 
16          $v_{\text{rec}} = \dot{s}_{\text{min}}$ 

17  if  $s_{\text{lead}} < s_{\text{safe}}$  and  $s_{\text{rear}} < s_{\text{safe}}$ 
18       $\dot{d}_{\text{max}} = 2a_{\text{max, lat}}$ 
19      if  $\dot{s}_{\text{min}} > \dot{s}_{\text{max}}$ 
20          $\dot{s}_{\text{max}} = \dot{s}_{\text{min}}$ 

Return:
    if DTT:  $\ddot{s}_{\text{dec, max}}, \ddot{s}_{\text{acc, max}}, \dot{s}_{\text{max}}, \dot{s}_{\text{min}}, \dot{d}_{\text{max}}$ 
    if FSPS:  $\ddot{s}_{\text{dec, max}}, \ddot{s}_{\text{acc, max}}, \dot{d}_{\text{max}}, v_{\text{rec}}$ 

```

Routine 1 shows the steps to obtain the kinematic constraints. Lines 1-6 imply that in the absence of a lead actor or a rear actor within the safety gap, the kinematic constraints should remain the same, which were determined prioritizing comfort. However, if there is a lead actor within the safety gap (line 7), then the maximum deceleration rate $\ddot{s}_{\text{dec, max}}$ is doubled (line 8) and the maximum velocity \dot{s}_{max} is constrained to lead actor's velocity v_{lead} (line 9). If the task is FSPS, the recommended speed v_{rec} is set to v_{lead} (line 11). Similarly, if there is a rear actor within the safety gap (line 12), the maximum acceleration rate $\ddot{s}_{\text{acc, max}}$ is doubled (line 13) and the minimum velocity \dot{s}_{min} is constrained to rear actor's velocity v_{rear} (line 14). With FSPS, the recommended velocity v_{ref} is set to \dot{s}_{min} if $v_{\text{ref}} < \dot{s}_{\text{min}}$ (line 16). In the event that there is both a lead and a rear actor within the safety gap (line 17), the lateral acceleration \dot{d}_{max} is doubled (line 18). Furthermore, the maximum velocity is adjusted in the event that the rear actor is moving faster than the lead actor (lines 19-20).

It is important to note that doubling both the lateral and longitudinal accelerations from the already given acceleration constraints is a heuristic for safety – the ego should be able to speed up its way out of danger in the event a lead or a rear actor breaches the safety gap without losing control. For example, with a higher lateral acceleration in effect, the ego can swerve away faster from the near-colliding vehicle, and this behavior is common in human drivers [39].

REFERENCES

[1] L. Claussmann, M. Revilloud, D. Gruyer, and S. Glaser, "A review of motion planning for highway

autonomous driving," *IEEE Transactions on Intelligent Transportation Systems*, vol. 21, no. 5, pp. 1826–1848, 2019.

[2] S. Karaman and E. Frazzoli, "Sampling-based algorithms for optimal motion planning," *The international journal of robotics research*, vol. 30, no. 7, pp. 846–894, 2011.

[3] T. Gu, J. Snider, J. M. Dolan, and J.-w. Lee, "Focused trajectory planning for autonomous on-road driving," in *2013 IEEE Intelligent Vehicles Symposium (IV)*. IEEE, 2013, pp. 547–552.

[4] M. McNaughton, C. Urmson, J. M. Dolan, and J.-W. Lee, "Motion planning for autonomous driving with a conformal spatiotemporal lattice," in *2011 IEEE International Conference on Robotics and Automation*. IEEE, 2011, pp. 4889–4895.

[5] Y. Huang, H. Ding, Y. Zhang, H. Wang, D. Cao, N. Xu, and C. Hu, "A motion planning and tracking framework for autonomous vehicles based on artificial potential field elaborated resistance network approach," *IEEE Transactions on Industrial Electronics*, vol. 67, no. 2, pp. 1376–1386, 2019.

[6] D. González, J. Pérez, V. Milanés, and F. Nashashibi, "A review of motion planning techniques for automated vehicles," *IEEE Transactions on intelligent transportation systems*, vol. 17, no. 4, pp. 1135–1145, 2015.

[7] A. Broggi, P. Medici, P. Zani, A. Coati, and M. Panciroli, "Autonomous vehicles control in the vislab intercontinental autonomous challenge," *Annual Reviews in Control*, vol. 36, no. 1, pp. 161–171, 2012.

[8] P. Petrov and F. Nashashibi, "Modeling and nonlinear adaptive control for autonomous vehicle overtaking," *IEEE Transactions on Intelligent Transportation Systems*, vol. 15, no. 4, pp. 1643–1656, 2014.

[9] L. Han, H. Yashiro, H. T. N. Nejad, Q. H. Do, and S. Mita, "Bezier curve based path planning for autonomous vehicle in urban environment," in *2010 IEEE intelligent vehicles symposium*. IEEE, 2010, pp. 1036–1042.

[10] M. Werling, J. Ziegler, S. Kammel, and S. Thrun, "Optimal trajectory generation for dynamic street scenarios in a frenet frame," in *2010 IEEE International Conference on Robotics and Automation*. IEEE, 2010, pp. 987–993.

[11] M. Geisslinger, F. Poszler, and M. Lienkamp, "An ethical trajectory planning algorithm for autonomous vehicles," *Nature Machine Intelligence*, vol. 5, no. 2, pp. 137–144, 2023.

[12] T. Stahl, A. Wischnewski, J. Betz, and M. Lienkamp, "Multilayer graph-based trajectory planning for race vehicles in dynamic scenarios," in *2019 IEEE Intelligent Transportation Systems Conference (ITSC)*. IEEE, 2019, pp. 3149–3154.

[13] S. Kammel, J. Ziegler, B. Pitzer, M. Werling, T. Gindele, D. Jagzent, J. Schröder, M. Thuy, M. Goebel, F. v. Hundelshausen *et al.*, "Team annieway's autonomous system for the 2007 darpa urban challenge," *Journal of Field Robotics*, vol. 25, no. 9, pp. 615–639, 2008.

- [14] M. Montemerlo, J. Becker, S. Bhat, H. Dahlkamp, D. Dolgov, S. Ettinger, D. Haehnel, T. Hilden, G. Hoffmann, B. Huhnke *et al.*, “Junior: The stanford entry in the urban challenge,” *Journal of field Robotics*, vol. 25, no. 9, pp. 569–597, 2008.
- [15] D. Ferguson, T. M. Howard, and M. Likhachev, “Motion planning in urban environments,” *Journal of Field Robotics*, vol. 25, no. 11-12, pp. 939–960, 2008.
- [16] Z. Han, Y. Wu, T. Li, L. Zhang, L. Pei, L. Xu, C. Li, C. Ma, C. Xu, S. Shen *et al.*, “An efficient spatial-temporal trajectory planner for autonomous vehicles in unstructured environments,” *IEEE Transactions on Intelligent Transportation Systems*, 2023.
- [17] X. Li, Z. Sun, D. Cao, D. Liu, and H. He, “Development of a new integrated local trajectory planning and tracking control framework for autonomous ground vehicles,” *Mechanical Systems and Signal Processing*, vol. 87, pp. 118–137, 2017.
- [18] X. Hu, L. Chen, B. Tang, D. Cao, and H. He, “Dynamic path planning for autonomous driving on various roads with avoidance of static and moving obstacles,” *Mechanical systems and signal processing*, vol. 100, pp. 482–500, 2018.
- [19] Y. Rasekhipour, A. Khajepour, S.-K. Chen, and B. Litkouhi, “A potential field-based model predictive path-planning controller for autonomous road vehicles,” *IEEE Transactions on Intelligent Transportation Systems*, vol. 18, no. 5, pp. 1255–1267, 2016.
- [20] N. Noto, H. Okuda, Y. Tazaki, and T. Suzuki, “Steering assisting system for obstacle avoidance based on personalized potential field,” in *2012 15th International IEEE Conference on Intelligent Transportation Systems*. IEEE, 2012, pp. 1702–1707.
- [21] X. Chen, Z. Huang, Y. Sun, Y. Zhong, R. Gu, and L. Bai, “Online on-road motion planning based on hybrid potential field model for car-like robot,” *Journal of Intelligent & Robotic Systems*, vol. 105, no. 1, p. 7, 2022.
- [22] I. Sung, B. Choi, and P. Nielsen, “On the training of a neural network for online path planning with offline path planning algorithms,” *International Journal of Information Management*, vol. 57, p. 102142, 2021.
- [23] Z. Huang, H. Liu, J. Wu, and C. Lv, “Differentiable integrated motion prediction and planning with learnable cost function for autonomous driving,” *IEEE transactions on neural networks and learning systems*, 2023.
- [24] L. Yang, C. Lu, G. Xiong, Y. Xing, and J. Gong, “A hybrid motion planning framework for autonomous driving in mixed traffic flow,” *Green Energy and Intelligent Transportation*, vol. 1, no. 3, p. 100022, 2022.
- [25] Á. Fehér, S. Aradi, F. Hegedűs, T. Bécsi, and P. Gáspár, “Hybrid ddp approach for vehicle motion planning,” 2019.
- [26] C.-J. Hoel, K. Driggs-Campbell, K. Wolff, L. Laine, and M. J. Kochenderfer, “Combining planning and deep reinforcement learning in tactical decision making for autonomous driving,” *IEEE transactions on intelligent vehicles*, vol. 5, no. 2, pp. 294–305, 2019.
- [27] H. Krasowski, X. Wang, and M. Althoff, “Safe reinforcement learning for autonomous lane changing using set-based prediction,” in *2020 IEEE 23rd international conference on Intelligent Transportation Systems (ITSC)*. IEEE, 2020, pp. 1–7.
- [28] PyTorch Geometric, “Heterogeneous graph learning,” [Online]. Available: <https://pytorch-geometric.readthedocs.io/en/latest/notes/heterogeneous.html>, Last Accessed: July 2023.
- [29] F. Scarselli, M. Gori, A. C. Tsoi, M. Hagenbuchner, and G. Monfardini, “The graph neural network model,” *IEEE transactions on neural networks*, vol. 20, no. 1, pp. 61–80, 2008.
- [30] J. Leskovec, “CS224W: Machine learning with Graphs, Stanford University,” [Online]. Available: <http://web.stanford.edu/class/cs224w>, Last Accessed: July 2023.
- [31] P. Veličković, G. Cucurull, A. Casanova, A. Romero, P. Lio, and Y. Bengio, “Graph attention networks,” *arXiv preprint arXiv:1710.10903*, 2017.
- [32] W. L. Hamilton, *Graph representation learning*. Morgan & Claypool Publishers, 2020.
- [33] PyTorch, “TORCH.FLATTEN,” [Online]. Available: <https://pytorch.org/docs/stable/generated/torch.flatten.html>, Last Accessed: February 2024.
- [34] O. Khatib, “Real-time obstacle avoidance for manipulators and mobile robots,” in *Proceedings. 1985 IEEE international conference on robotics and automation*, vol. 2. IEEE, 1985, pp. 500–505.
- [35] S. Aradi, “Survey of deep reinforcement learning for motion planning of autonomous vehicles,” *IEEE Transactions on Intelligent Transportation Systems*, vol. 23, no. 2, pp. 740–759, 2020.
- [36] P. A. Lopez, M. Behrisch, L. Bieker-Walz, J. Erdmann, Y.-P. Flötteröd, R. Hilbrich, L. Lücken, J. Rummel, P. Wagner, and E. Wießner, “Microscopic traffic simulation using sumo,” in *2018 21st international conference on intelligent transportation systems (ITSC)*. IEEE, 2018, pp. 2575–2582.
- [37] The MathWorks Inc., “Navigation toolbox version: 2.3 (r2022b),” 2022. [Online]. Available: <https://www.mathworks.com/help/stats/index.-html>
- [38] N. Hogan and D. Sternad, “Sensitivity of smoothness measures to movement duration, amplitude, and arrests,” *Journal of motor behavior*, vol. 41, no. 6, pp. 529–534, 2009.
- [39] X. Li, A. Rakotonirainy, and X. Yan, “How do drivers avoid collisions? a driving simulator-based study,” *Journal of safety research*, vol. 70, pp. 89–96, 2019.



Jilan Samiuddin received his B.Sc. degree in Electrical and Electronic Engineering from American International University - Bangladesh and M.Sc. degree in Electrical Engineering from the University of Calgary in 2012 and 2016, respectively. He is currently a Ph.D. candidate in the Department of Electrical and Computer Engineering at McGill University. His research is primarily focused on machine learning algorithms with the motivation of developing novel strategies for autonomous driving.



Di Wu is a senior staff research scientist, a team leader at Samsung AI Center Montreal and an Adjunct Professor at McGill University since 2019. He did postdoctoral research at Montreal MILA and Stanford University. He received his Ph.D. and M.Sc. from McGill University in 2018 and Peking University in 2013, respectively. Di also holds Bachelor's degrees in microelectronics and economics. His research interests mainly lie in reinforcement learning, transfer learning, meta-Learning, and multitask Learning. He is also interested in leveraging such algorithms to improve real-world systems.



Benoit Boulet, P.Eng., Ph.D., is Professor of Electrical and Computer Engineering at McGill University which he joined in 1998, and Director of the McGill Engine. He is also McGill's Associate Vice-President (Innovation and Partnerships). Prof. Boulet obtained an M.Eng. degree from McGill in 1992 and a Ph.D. degree from the University of Toronto in 1996, both in electrical engineering. He is a former Director and current member of the Centre for Intelligent Machines where he heads the Intelligent Automation Laboratory. His research interests include the design and data-driven control of autonomous electric vehicles and renewable energy systems and applications of machine learning.